



A New Hybrid Friction Damper (HFD) for Dual-Level Performance of Steel Structures

Babak Shahbazi¹ · Elham Moaddab¹

Received: 10 January 2021 / Accepted: 17 June 2021 / Published online: 7 July 2021
© Korean Society of Steel Construction 2021

Abstract

In this study, a new hybrid energy dissipation device is developed by combining two friction dampers (auxiliary and main fuse) in series to be used for the seismic control of two different earthquake intensities. Compared with the conventional friction dampers, the new hybrid damper has an advantage in that only the auxiliary fuse (with low sliding force) is activated for moderate earthquakes and both fuses work simultaneously for strong earthquakes. Cyclic loading tests of the combined hybrid dampers are carried out to evaluate their seismic energy dissipation capability. The obtained experimental force displacement indicates proper details of the new damper to create two performance levels. Finite element analyses of the test specimens are also carried out for comparison and have good agreement with the test results. Force–displacement characteristics, energy dissipation, and equivalent viscous damping are also derived and good agreement has been found. Moreover, it is demonstrated that by engaging the main fuse with non-loaded pretension bolts, the strength losses of the hybrid damper in the subsequent cycles are limited compared with the common friction dampers, which can be called the “resurrection-type” behavior of the main fuse in the main shocks. To evaluate the effects of the proposed damper, typical 3- and 9-story steel buildings are modeled and their seismic responses under 22 earthquake excitations are investigated using incremental dynamic nonlinear time-history. Comparison of incremental dynamic analysis (IDA) curves and their medians revealed that using a hybrid friction damper (HFD) reduces the probability of reaching all the defined damage states. Moreover, the reduction effect of HFD was recognizable in 9-story frames.

Keywords Hybrid damper · Friction · Moderate earthquakes · Severe earthquakes · IDA analysis

1 Introduction

Response control of structures is one of the reliable approaches to increase the safety and stability of structures against wind and earthquake excitation. Passive, active, and semi-active controls are the main classes of structural control systems. The passive systems, also known as passive energy dissipation devices, do not require an external source of power; therefore, they have been considered an effective and common way to decrease the effect of earthquakes on structures. In passive control systems, the input energy supplied by wind and/or earthquake can be dissipated within energy dissipative devices through yielding or friction (Soong & Spencer, 2002). Several comprehensive references

are available on the behavior, analysis, and design of passive systems (e.g., Hanson & Soong, 2001; Ibrahim et al., 2007; Marshall and Charney, 2010). Variety and flexibility of passive control devices have result in their versatile applications in structures. Bazzaz et al., (2012, 2014) proposed the use of yielding ring damper in off-center brace systems to increase the ductility of braces. Numerical and experimental studies revealed that in addition to simple construction technology of ring dampers, they resulted in more ductility, high performance and easy replacement of damaged member after hazardous earthquake (Andalib et al., 2014, 2018; Bazzaz et al., 2015).

Since the growth of using dampers in structures, design requirements in available seismic codes have been considered. Different approaches to design displacement-dependent devices have revealed that design earthquake levels are selected based on severe earthquakes (ASCE & SEI41–13, 2010; ASCE & SEI7–10, 2010). The level of excitation determines the start of the energy-absorbing process in

✉ Elham Moaddab
e.moaddab@seraj.ac.ir

¹ Department of Engineering, Seraj Higher Education Institute, Tabriz, Iran

dampers. Based on design codes, displacement-dependent dampers are designed to remain elastic during moderate earthquakes and their function is postponed to the times when severe earthquakes occur. These dampers show elastic behavior below the yield load and produce a minimal amount of energy dissipation, which makes them ineffective in a weak earthquake or a wind load. The elastic behavior of dampers in severe excitations increases the stiffness of the whole structure in low-level and moderate earthquakes and leads to imposing high base shear or structural element forces.

More recently, some efforts have been made to overcome this problem by combining various energy dissipation devices. Simultaneous application of multiple devices maximizes the energy dissipation mechanism in major and minor earthquakes or wind-induced excitations. The hybrid configuration of dampers has been investigated by Smith and Wilford (2007). Their proposed hybrid dampers included viscoelastic dampers and buckling-restrained braces (BRBs) to control wind and earthquake excitations in one device. Kim et al. (2009) introduced a hybrid BRB (H-BRB), which improved the performance of the BRB, as a type of composite damper system consisting of a BRB and a viscoelastic damper. The result of the time-history analysis showed that H-BRB is effective in improving both the lateral stiffness and the serviceability of a building using the existing damper. Moreover, the effect of the proposed damper on the seismic response of structural systems was investigated in another study (Kim et al., 2014). Karvasilis et al. (2011) assembled compact elastomer materials with different properties as a hybrid damper to control the seismic response of structures in different displacement amplitudes. Ibrahim et al. (2007) studied the combination of yielding dampers and viscoelastic dissipation devices. In this combination, low excitement (wind) was controlled by the viscoelastic damper and high-level excitement was damped through the yielding part. Marshall and Chareny (2010) experimented with a high-damped rubber in series with a BRB as one seismic control device. In another investigation, Lee et al. (2016) combined a friction damper and a steel strip damper to improve the seismic performance of structures at multiple levels of ground motion. Experimental evidence demonstrated that the fatigue life of the steel strip part was enhanced by simultaneously using the friction damper. More recent studies have been completed by combining multiple ring dampers (Cheraghi and Zahraie, 2016) and the dual-performance triangular-plate added damping and stiffness (TADAS) damper (Hosseini & Moaddab, 2017).

Several studies have shown that combining rate-dependent and displacement-dependent dampers reduces the effectiveness of the latter (Symans et al., 2008). In addition, evidence has clarified that assembling displacement-dependent dampers with gap displacement needs more accuracy, and

not considering the exact displacement distance between two fuses leads to an unwanted increase of stiffness in the damper (Hashemi & Moaddab, 2017).

The purpose of this study is to develop a hybrid friction damper (HFD) that works for both major and minor earthquakes numerically and experimentally. The developed hybrid damper consists of a two-part friction damper named here with main and auxiliary fuses to resist strong and small earthquakes, respectively. The auxiliary and main fuses are connected through a displacement gap (horizontal holes) in series. The auxiliary friction part consists of a friction damper with low pretension force on bolts and the main part is provided with high pretension force which is designed based on severe earthquakes. Cyclic loading tests of the hybrid dampers are carried out to evaluate their seismic energy dissipation capability. The hybrid dampers are applied to the seismic retrofit of an analysis model structure, and the effectiveness of the dampers is assessed using incremental dynamic analyses (IDAs) to obtain the probability of reaching four limit states.

2 Development of a Hybrid Friction Damper

The hybrid damper developed in this study consists of two sets of friction damper unit to resist strong and moderate earthquakes separately. The friction sets are connected in series as a single energy dissipation device as shown in Fig. 1 schematically. Two friction parts active separately due to their different slip force, low slip force for moderate earthquakes and high slip force in second part for severe earthquakes. To assemble each friction unit, two friction plates (thickness: 2 mm each), two steel plates (thickness: 10 mm each), an inner steel plate (thickness: 15 mm) were tightened with an M12.9 high-tension bolts. The diameter of used bolts was 20 mm. Two separate friction parts have been

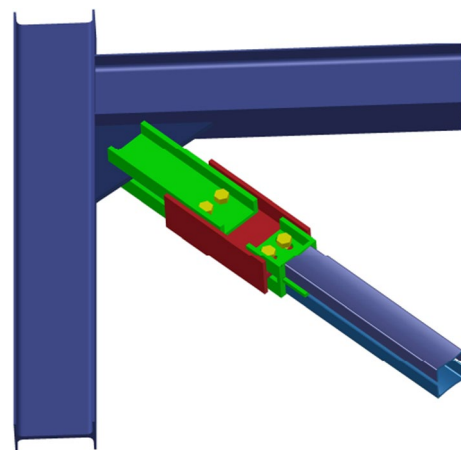


Fig. 1 Overall view of introduced hybrid friction damper

attached to a single friction plate. As detailed in Fig. 2 each part has their own pretention bolts which can produce different level of slip forces. Plate B (inner steel plate of 15 mm thickness) connects fuse one and two which enable them to act as a single device. The horizontal slotted holes provided the displacement gap needed for both dampers in such a way to involve the second friction part as the main fuse in the system. Also, slotted holes in second fuse have been considered longer than first fuse's one in order to provide main fuse to move freely during any occurred displacement in major earthquakes. Amplitude of horizontal slotted holes have been considered 15 mm based on corresponding displacement amplitude in moderate earthquakes (1% interstory drift ratio). In severe earthquakes, with high displacement demand more than 1% amplitude, the pretention bolts in first fuse attached to the end of horizontal slotted holes and force transfers to the main fuse. So the whole length of horizontal slotted holes was considered equal to 50 mm with 20 mm diameter high tension bolt in half scale.

To evenly distribute the clamping force on the surface of the friction pads, the rectangular plates are inserted between the bolt head or the nut and the steel side plates. Brass plates Half cartridge (UNS-260) type have been used to provide sufficient friction coefficient between two moving plates. The maximum installation axial force for each high tension bolt was 70 kN, and thus the target total frictional force of each damper (i.e., the sum of the forces of the two friction units) was 140 kN. A preliminary test of friction damper units was conducted to obtain the relationship between the slip load and pretention torque. Based on this result, the friction coefficient between the friction pads and steel plates was determined approximately 0.3.

A torque meter device was applied to measure and adjust the needed pretention force in each part of damper. Four specimen have been tested under cyclic loading according to details in Table 1.

3 Experimental Study

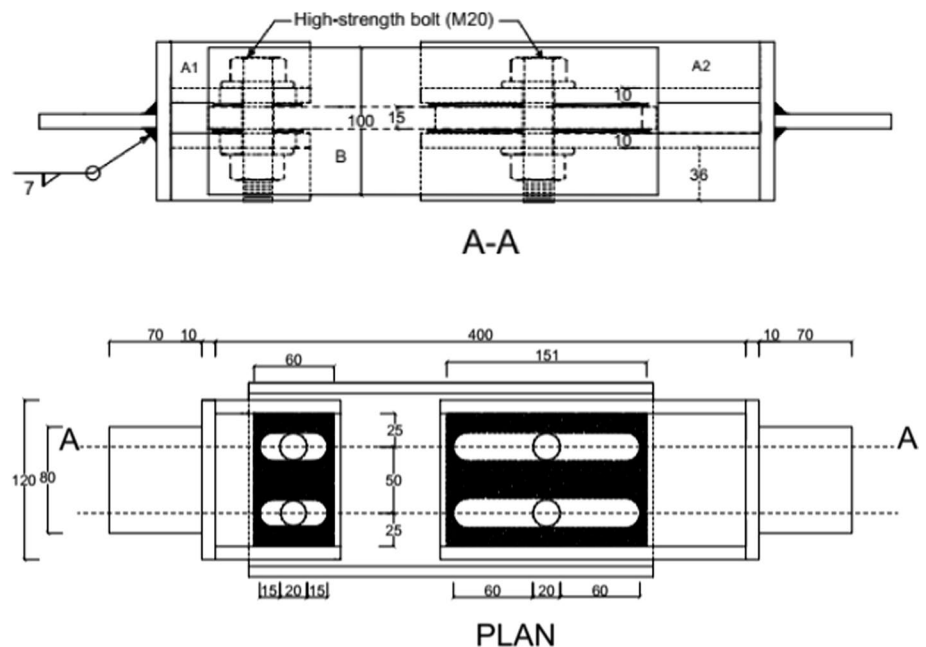
3.1 Loading Protocol

Axial tests were performed in order to determine the hybrid friction damper (HFD) displacement-force curve at the displacement amplitudes according to the allowed drifts at the LS performance level. The HFD test is performed in accordance with the protocols of ASCE/SEI41 (2010) for displacement devices. Accordingly, a cyclic quasi-static test with 20 cycles of displacement have been carried out on the samples and the hysteresis behaviour of the HFD have been studied under two different sliding force for different slipping phases at 0.1 Hz. The applied displacement amplitudes were selected in such a way that both the auxiliary and main fuses interfered in the total force recorded. Therefore, as shown in Table 1, the imposed displacement amplitude

Table 1 Sliding force of hybrid damper

Sample	P_{S1}	P_{S2}	P_{S2}/P_{S1}	δ_{max} (mm)
A	15	28	1.9	50
B	36	104	2.9	40
C	60	180	3	60
D	87.5	237	2.7	60

Fig. 2 Detail of tested hybrid friction damper



(δ_{\max}) are greater than 15 mm. A total 20 loading cycles with constant amplitude of displacement δ_{\max} have been applied to experimental samples.

3.2 Set Up

As illustrated in Fig. 3, the hybrid friction damper (HFD) sample was placed vertically in the universal device with a capacity of about ± 500 kN, a displacement range of 500 mm, and a maximum velocity of 100 mm/s. The test device also was equipped with a 900-kW load cell and a linear variable displacement transducer (LVDT) that records the force–displacement ratio for each step. The experiments were conducted in the Material Strength Lab of Seraj Institute of Higher Education.

The initial sliding forces for the HFD-A hybrid dampers were adjusted to 15 and 28 kN for the main and auxiliary fuse, respectively. The first test carried out on sample A to ensure achieving two level performance of proposed damper. Value of sliding force in sample B to D have been increased regarding the universal loading device capacity limitation. It should be noticed that the sliding force value can be adjusted in practical use based on structural element characteristics. The calibration coefficient can be calculated by assuming a suitable value of friction coefficient; i.e., 0.3.

3.3 Experimental Results

The relevant test results were used to plot hysteresis curves for the HFD in Fig. 4. In the mentioned diagrams, energy is dissipated by an auxiliary fuse of the HFD damper



(a) Experimented sample



(b) set up of hybrid friction damper

Fig. 3 Experimental study

before 15 mm displacement amplitude, and then the second phase (main fuse) continues until further displacements occur. As observed in the force–displacement curve in subsequent experiments, to achieve greater energy dissipation by the HFD, the sliding force was increased in both auxiliary and main fuses. The increase in the force associated with gap displacement is evident in the hysteresis curves of the tested samples. For example, for sample "A", the auxiliary fuse force is about 18 kN before reaching the gap displacement enhanced to 34 kN when the main fuse is engaged. In all the tested specimens, the tolerated force has increased after gap displacement. To investigate the effect of energy dissipation of the main fuse in the samples, the range of the imposed displacement was selected to be at least twice the gap displacement. Maximum force and imposed displacements are described in Table 1 for all the experimental results.

At higher reversal cycles in the tested specimens, the slippage force drops those results in a decrease of the force of the damper. It has been observed that the force reduction is compensated by adding the unloaded main fuse to the auxiliary one in higher displacement demands. The added fuse as the main fuse has not been subjected to a cyclic load and is used as a source of new energy dissipation whose capacity has not been used. Based on multilinear curves, the effective parameters including the slip force for both compressive and tensile forces were obtained as reported in Table 2, where P_{s1} and P_{s2} are the slipping forces of the auxiliary and main fuses, respectively. The values of the forces reported are slightly different from the maximum values of the forces recorded in the laboratory results. The main cause for such a difference is the slip force reduction in cycles. The slip load of the hybrid damper decreases along with the cycles; however, this reduction is within the acceptable range according to the requirements of ASCE /SEI41 (2010). According to this specification, in each test, the slip force obtained in each full loading cycle must not differ from the average calculated slip load by more than 15% for all the cycles of that test. Based on the resulted force–displacement curves, the maximum deviation from the slip load criterion was obtained from the first cycle of the B test, which is equal to 11%.

For practical cases, it is preferred to present the damper characteristics with equivalent viscous damping values. Accordingly, an effective one-degree-of-freedom of stiffness is expressed as follows (FEMA356, 2000).

$$K_{\text{eff}} = \frac{|F^+| + |F^-|}{|\Delta^+| + |\Delta^-|} \quad (1)$$

where $+F$ and $-F$ forces are obtained at the maximum displacement of $+\Delta$ and $-\Delta$, respectively. Similar to the slip

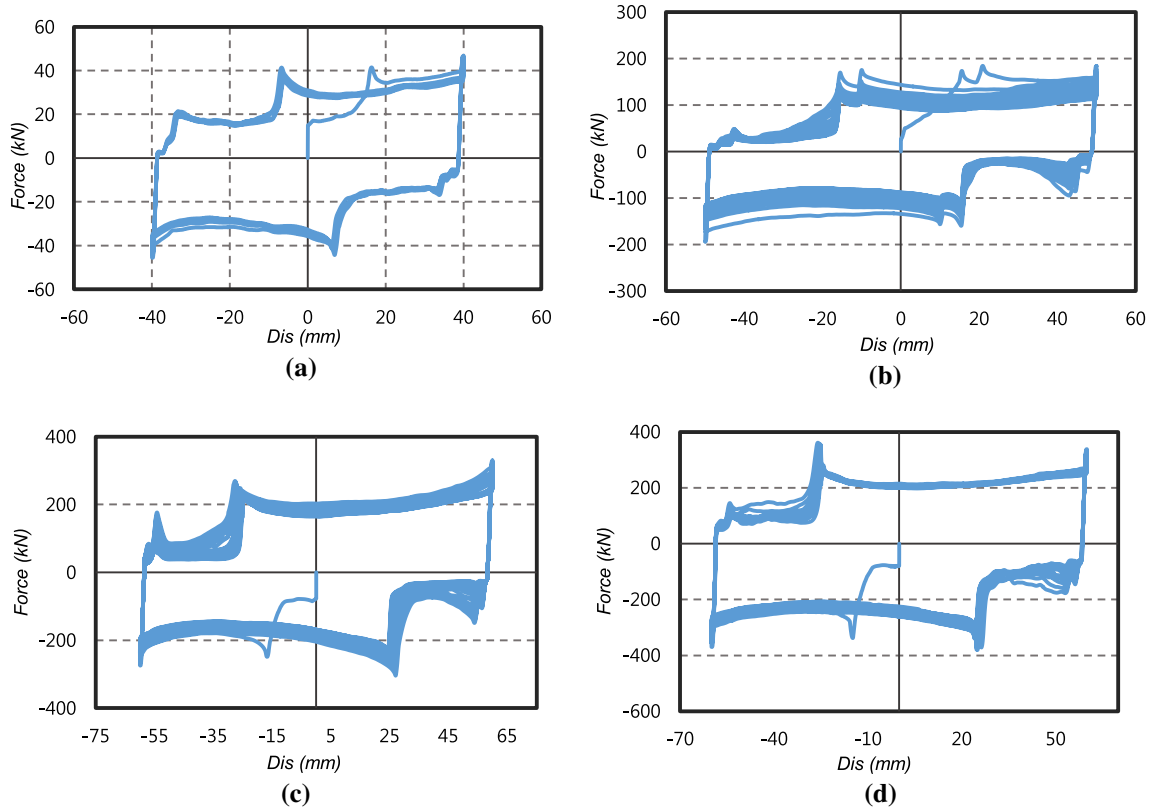


Fig. 4 Cyclic test results for sample A to D

Table 2 Results of experimental study of samples based on multi linear force–displacement curves

Sample	A	B	C	D
P_{s1}^*	18	43	72	105
P_{s2}^*	34	125	217	285

* P_{s1} : slip force of auxiliary fuse; P_{s2} : slip force of main fuse

force, according to ASCE/SEI41 (2006), in each test, the effective stiffness of an energy dissipation device per cycle for damping must not differ $\pm 15\%$ between all the cycles of that test, as compared to the average calculated stiffness.

The tested dampers A and D show the lowest and highest effective stiffness values, respectively as seen in Fig. 5.

The energy dissipation in each cycle, W_D , should be considered as the area surrounded by a complete cycle of the displacement force response. According to the ASCE/SEI41 (2010) guideline, the area within the hysteresis cycle (W_D) of an energy dissipation device should not differ more than $\pm 15\%$ relative to the average area under the cycle curve between all cycles of that test. According to the obtained results, the maximum mean deviation is related to the first cycle of test B, which is equal to 10%.

In Fig. 6, a cumulative energy dissipation diagram is presented against the loading cycle for tests A to D. It is

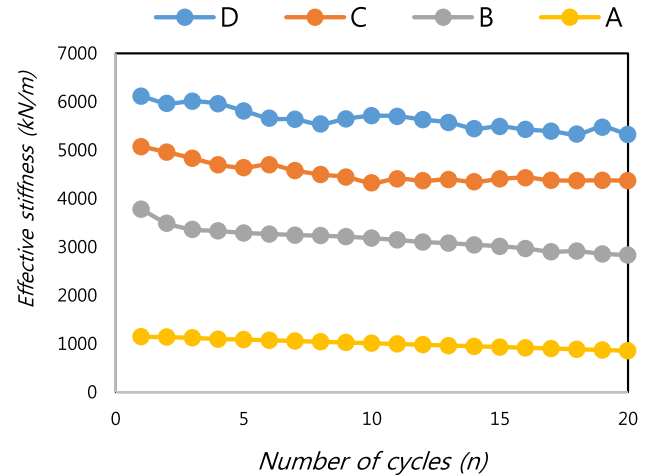


Fig. 5 Calculated effective stiffness for experimental samples

evident that the slope of the energy dissipation diagram increases with increasing slip force.

Viscous damping ratio has been defined by FEMA356 (2000) to determine the equivalent viscous damping for structural members. This coefficient is expressed by the following equation:

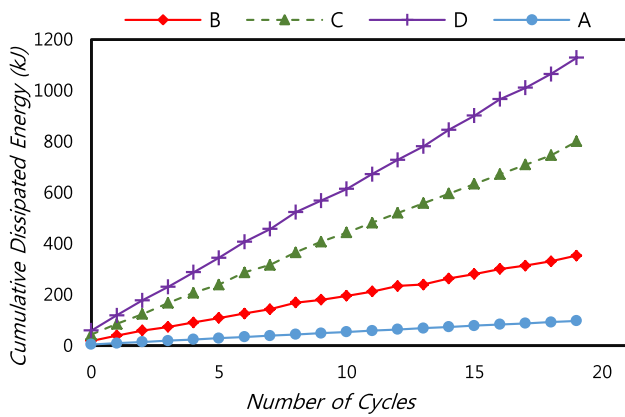


Fig. 6 Cumulative dissipated energy for tested samples of hybrid friction damper

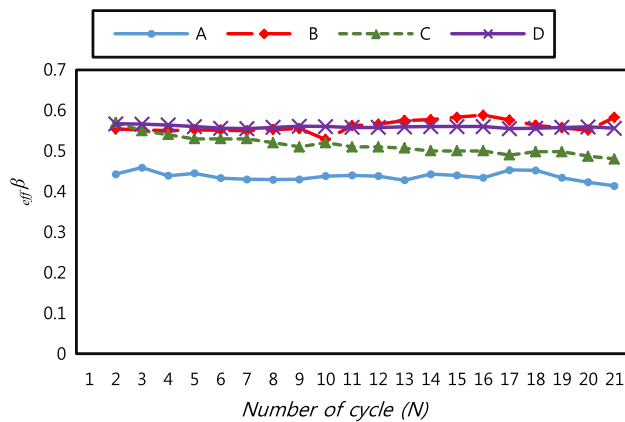


Fig. 7 Equivalent viscous damping for tested samples of hybrid friction damper

$$\beta_{\text{eff}} = \frac{1}{2\pi} \frac{1}{k_{\text{eff}}} \frac{W_D}{\Delta_{\text{avr}}^2} \quad (2)$$

where Δ_{avr} is equal to the mean absolute values of the displacements $+\Delta$ and $-\Delta$. Also, k_{eff} is the effective stiffness and W_D is the value of energy absorbed. The mean value of β_{eff} for samples is estimated to be about 0.55 for all samples (Fig. 7).

4 Numerical Study

4.1 HFD Component Numerical Model

A numerical analysis was performed using OpenSees software to obtain the numerical cyclic behaviour of the HFD. Each section of the damper is modelled using a hybrid link element with perfect elastoplastic behaviour. Additional energy absorption may be carried out through other sources

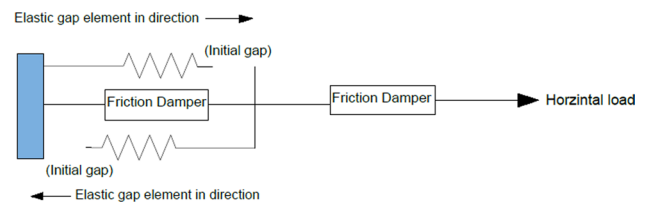


Fig. 8 Schematic view of numerical model of hybrid damper in open-sees

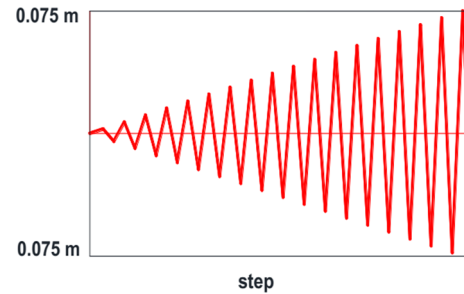


Fig. 9 Loading protocol of numerical models

such as power transmission bolts, which are expected to remain elastic and rigid. During the experiments, no apparent permanent deformation was observed in the holding bolts; therefore, the force transmission elements are considered rigid with elastic properties.

In Fig. 8, the ideal numerical model of a hybrid damper is illustrated. The horizontal force P reaches the endpoint, with x -degree of freedom. Each part of the hybrid damper was modelled with a zero-length element with perfect plastic material specifications. Element displacement force behaviour is presented with a bilinear diagram. The force is determined through three parameters of initial stiffness, stiffness after yielding (defined as the ratio of stiffness after yielding to the initial stiffness), and slip load. These parameters must be adjusted so that the rectangular shape of the hysteresis loops is achieved for friction behaviour. To consider the lagged displacement function, the Gap-Hook element was used in two loading directions as compressive and tensile. Different slipping forces of the main and auxiliary fuses were created given the different yielding forces for two materials with EPP specifications.

In the component parametric study, a load pattern different from the one used in laboratory studies was applied. Figure 9 shows the amplitudes of the applied deformations on numerical models. The increasing range of displacements in numerical studies was chosen to represent the independent effects of the first fuse in the elementary cycles.

The experimental results were verified using the hybrid model described for sample B in the OpenSees software. The

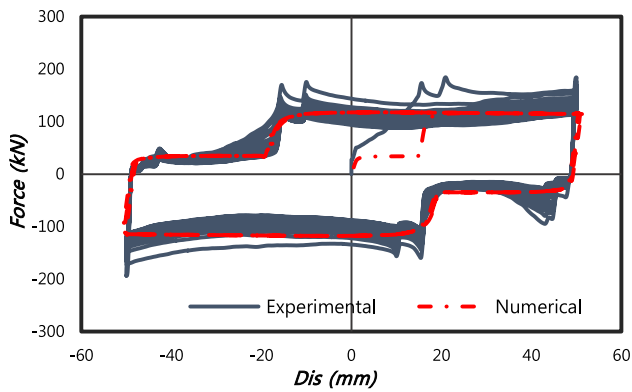


Fig. 10 Verification of numerical model

Table 3 Numerical models of hybrid damper properties

Model	P_{S1} (kN)	P_{S2} (kN)	P_{S1}/P_{S2}	P_{S2}/P_{S1}
a	93	172	0.54	1.85
b	74	165	0.45	2.23
c	70	200	0.35	2.86
d	55	230	0.24	4.18
e	45	268	0.17	5.6
f	35	297	0.12	8.5
g	93	345	0.27	3.7
h	70	270	0.26	3.86
i	50	185	0.43	3.7
j	35	143	0.24	4.1

initial stiffness of the tangent gradient in the loading vector was assumed to be 10,000 N/m and 20,000 N/m for the main and auxiliary fuses, respectively.

Figure 10 illustrates the force–displacement results obtained from the hybrid model in the software in comparison with the experimental results of sample B. The resulting dual-level cyclic curve shows that the selected hybrid elements can perfectly capture the overall cyclic behaviour of the HFD. Comparison of the results obtained for model B with the slip force values of 43 and 125 kN and those obtained from the numerical model in OpenSees software indicates a reasonably good agreement.

4.2 Parametric Numerical Component Studies

To simulate the cyclic behaviour of friction hybrid dampers, the finite element model of the damper was created using the OpenSees software (Opensees, 2014). According to the loading protocol shown in Fig. 9, the sample of the finite element model was created and loaded under increasing cyclic loading to the range of 75 mm. Table 3 represents the parametric characteristics, including the main fuse displacement lag (Δ_{gap}), slip forces P_S , their ratio, and the final displacement applied

to the damper (δ_{max}). The slip forces were chosen so that different ranges of slip force ratios (P_{S1}/P_{S2}) could be achieved in two phases in order to examine the effect of this parameter on energy absorption or the equivalent damping value.

Figure 11 presents the results of numerical component models with different slip loads for models (a) to (j) under cyclic loading with increasing displacement amplitudes. In Figs. 12, 13, 14, 15, the values of cumulative energy dissipation, effective stiffness, and equivalent viscous damping have been compared for the mentioned numerical models. Since the loading protocols are the same for all the models, the value of cumulative energy dissipation was changed with respect to the slip force in each model. Energy dissipation is mostly identical in all the models in the initial cycles due to their small displacement amplitudes. Conversely, by increasing the displacement amplitudes at higher cycles, an ascending rate of energy dissipation is observed with an increase in the slip force. Model (g) with a greater slip force has the maximum energy dissipation for subsequent cycles.

The resulting trend of effective stiffness in all the models demonstrates that the stiffness goes up due to an increase in the slip force. However, in the subsequent cycles, larger imposed displacement amplitudes result in a decrease in the stiffness values. These changes indicate that the stiffness of the damper imposed on the structure decreases as slipping begins and is reduced with an increase in the displacement range experimented by the damper.

The equivalent damping ratio was calculated for each cycle in numerical models given the area of force displacement. Figure 14 demonstrates the equivalent damping variation in different numerical models with different slip forces against loading cycles. In the initial cycles, due to the small range of input displacement, the calculated damping is not significant; however, by increasing the range at higher cycles and adding the slip force in the main fuse, the equivalent damping value (especially in displacements greater than 15 mm) is enhanced. Eventually, the damping value in the last loading cycles reached 0.51.

Figure 15 shows the maximum absorbed energy versus the changes in the ratio of the slip force forces (P_{S1}/P_{S2}) for all models. The general trend observed in this diagram confirms that by increasing the ratio of slip force, the energy absorption value increases, as well. Nevertheless, it is not possible to judge this case by considering the damper alone; instead, the value of energy absorbed by the damper must be compared in structures with a hybrid damper and common damper, especially in moderate earthquakes.

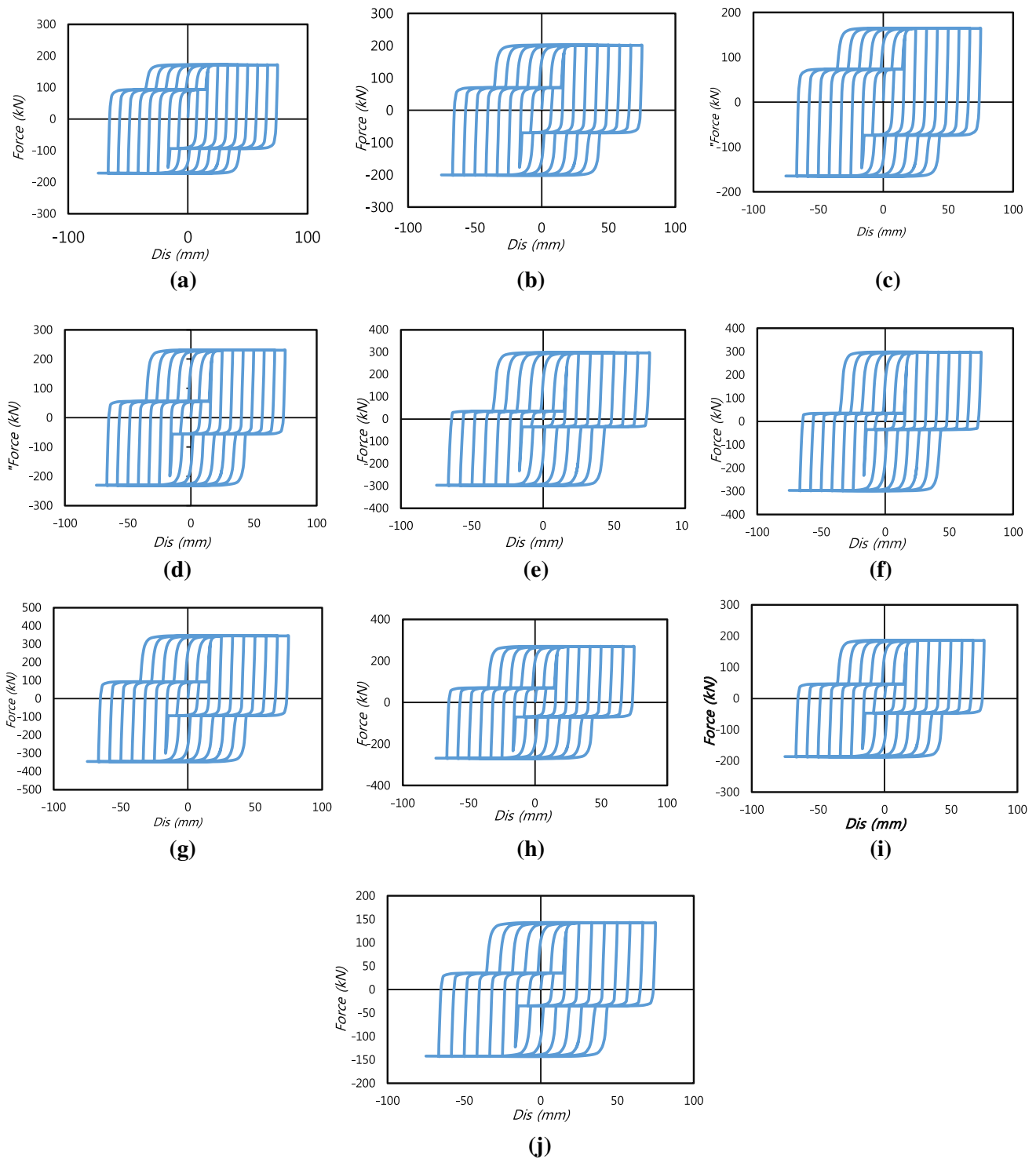


Fig. 11 Force displacement cyclic curve of numerical component models a to j

4.3 Seismic Evaluation of HFD Equipped Frames

4.3.1 General Specifications of the Frames

To explore and compare how the hybrid friction damper

affects the seismic performance of structural frames, structural frame equipped by common friction damper and hybrid friction damper have been analyzed. Two sets of three and nine story frame that as a part of SAC Project (FEMA350, 2000; FEMA356, 2000) are selected for the numerical

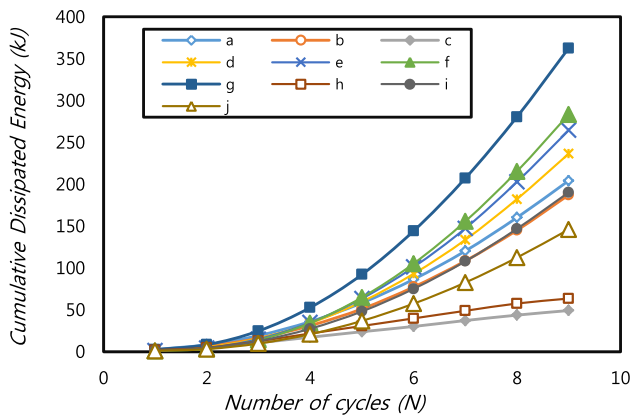


Fig. 12 Cumulative dissipated energy versus number of cycles in component numerical models

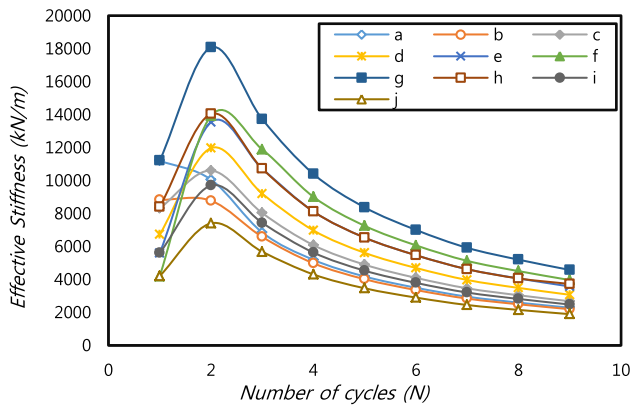


Fig. 13 Effective stiffness variation versus number of cycles in cycles in component numerical models

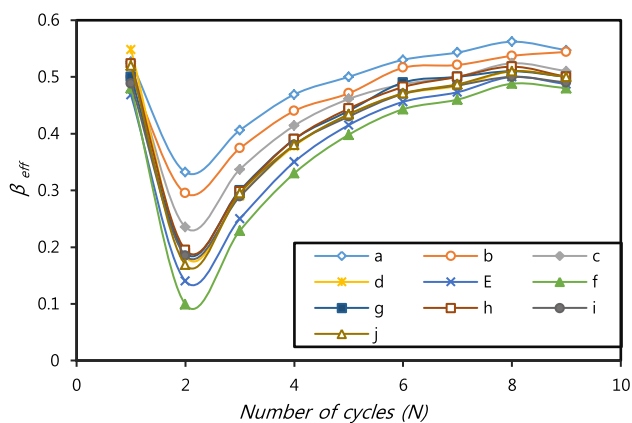


Fig. 14 Effective stiffness variation versus number of cycles in cycles in component numerical models

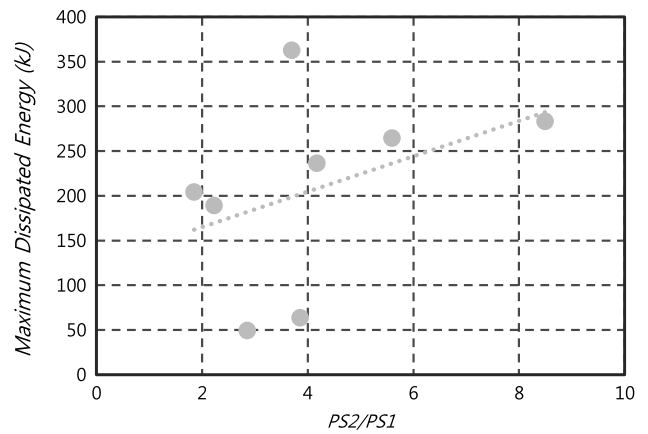


Fig. 15 Effect of first and second fuse slip force ratio on maximum dissipated energy

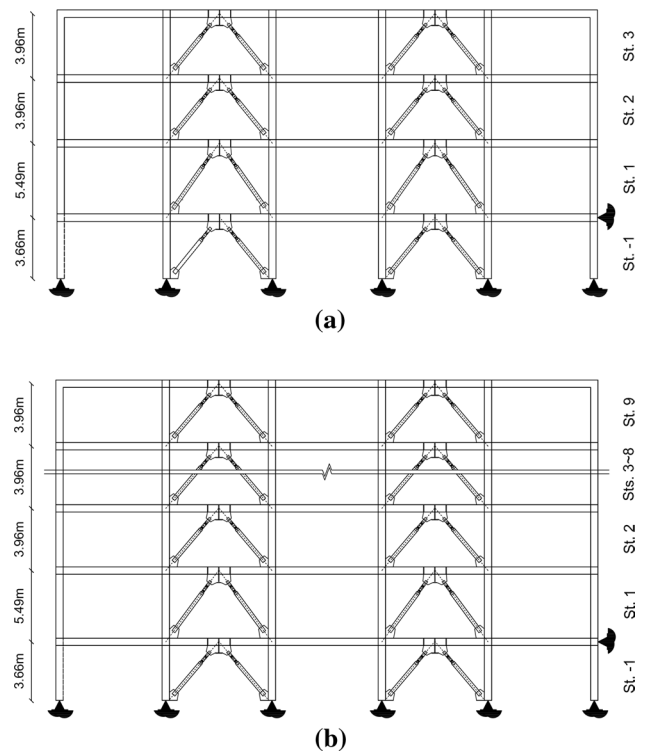


Fig. 16 Frames geometry and the locations of friction and hybrid friction dampers: **a** 3-story, **b** 9-story

studies. For this purpose, one of the perimeter frames in the E-W direction of SAC building are selected for the design. All the geometrical dimensions, the gravity loading and the seismic mass on the frames conform to the SAC models as shown in Fig. 16. In the original SAC frames, typically, inter-story drift limits govern the beams and columns sections sizes. The dampers were added to these frames and all beams and columns sections were re-designed to conform to ASCE 7-10 (2010) requirements for structural

systems with dissipative friction devices. The beams, columns and braces sections for each frame type is shown in Table 4 represents design specifications of both friction and hybrid friction dampers per story of each frame. The yielding and ultimate stresses and the Poisson ratio of the steel material are 235 MPa, 370 MPa and 0.3, respectively. The design spectra conforms to the Iranian Seismic Design Code (BHRC, 2015) for a site of high seismicity locating on a Soil Type III soil (similar to Soil Class D per ASCE 7-10 (2010) (Table 20.3-1)).

The Open Sees program (OpenSees, 2014) is used to develop the numerical model of the structural frame models as illustrated in Fig. 16. Concentrated plasticity have been assigned to the beams and columns at their ends in numerical model. Their hysteretic response deteriorates based on the modified Ibarra–Krawinkler model (Ibarra et al., 2005). Nonlinear geometry for both beam and column is also activated to account the second-order effect. As mentioned before, in component modelling section, each part of the hybrid damper was simplified through zero-length elements with a uniaxial material property connecting the end of braces to column beam joint, while elastic truss element is implemented to model the braces. More specifically, ElasticPP (elastic–perfectly plastic) material was used to model FD, and ElasticPP Gap (elastic–perfectly plastic gap) material was used to make an initial gap in the friction unit so that sliding motion could occur. A uniform distribution of dampers with slip force at each floor is assumed equal to 218 kN and 114 kN for friction damper and hybrid friction damper for 9 story building respectively. These values have been set for 3 story building equal to 185 and 110 kN for friction damper and hybrid friction damper building respectively.

4.3.2 IDA of Model Structures

In this study, incremental dynamic analyses are conducted to obtain seismic fragility of structural frames (damped

structures) by using suite of twenty scaled far-field records prescribed in FEMA P695 (FEMA, 2009) presented in Table 5. In applied incremental dynamic analysis, the scale factors from 0.1 g up to 4.0 g are chosen to both systems, with an accelerations interval of 0.1 g. The scaled ground motions are applied to the structure to cover seismic behavior in elastic and plastic regions and capture the collapse capacity of structure. The results are represented by maximum acceleration as intensity measure versus structural response (interstory drift). According to FEMA 350 (2000), damage states describe structure damage states for seismic loads and are classified into collapse prevention, life safety and immediate occupancy. In this study, the IO, LS, and CP are defined when inter-story drift ratio reaches 1%, 2% and 4% of the floor height, respectively. Also collapse of structures can be defined when dynamic instability of structures occurs in half of records or state of dynamic instability is defined as the point at which the stiffness decreases lower than 20% of the initial stiffness in the incremental dynamic analysis.

Figure 17 shows the incremental dynamic analysis results of the model structures for both frames with common friction damper and hybrid friction damper. From Fig. 17 it can be concluded that all the IDA curves have a linear part which shows elastic behavior and followed by a nonlinear part as a sign of inelastic behavior. In the inelastic region, the IDA curves display the stiffness degradation or a softening behavior until the structures collapse takes place. Due to the inherent uncertainty of ground motions, the scattering and variability of IDA curves can also be observed so it is important to use the statistical method for evaluation. In this paper, the 16th, 50th and 84th fractile values of IDA curves are calculated (Fig. 18) and summarized in Table 6 to evaluate the seismic behavior of structures. It can be observed that the median spectral acceleration at dynamic instability increases from 1.3 g in the 3-story structure with common friction damper to 1.8 g in the structure with hybrid dampers. Even though the common friction damper and the hybrid dampers have the same strength, the median failure accelerations of the structures with hybrid dampers are slightly higher than those of the structures with common friction dampers. The increase of median spectral acceleration from 0.5 g to 1.0 g has been highlighted in 9-story frames.

As reported in Table 6 the maximum acceleration corresponding to the 50% probability (the median structural capacity) of reaching the CP damage state turns out to be highest value of 1 in the 9-story structure equipped by hybrid friction damper whereas this value decrease to 0.5 in 9th-structure with common friction damper. This implies that for a given acceleration the probability of reaching the CP limit state is lowest in the structure using hybrid dampers. The probabilities of reaching the LS and IO damage state show similar trend, except that the difference between the

Table 4 Design specifications of the frames elements: (a) 3-story model (b) 9-story model

Story	Beams section	Exterior columns sections	Interior columns sections	Braces sections
<i>(a)</i>				
0 to 1	W36X160	W14X370	W14X455	2C5X9
1 to 2	W36X135	W14X283	W14X370	2C4X7.25
2 to 3	W30X99	W14X257	W14X283	2C4X7.25
<i>(b)</i>				
– 1 to 3	W36X160	W14X370	W14X455	2C7X12.25
3 to 6	W36X135	W14X283	W14X370	2C6X10.5
6 to 7	W30X99	W14X257	W14X283	2C6X10.5
7 to 9	W27X84	W14X233	W14X257	2C5X9

Table 5 Selected strong ground motion records utilized in this study

Record no	Record ID mean	Components IDs according to PEER NGA database (PEER, 2015)		PGAcomponent-1 (g) 2.53	PGAcomponent-2 (g) 3.34	Normalization factor 2.67
		Component 1	Component 2			
1	953	NORTHR/MUL009	NORTHR/MUL279	0.52	0.42	0.65
2	960	NORTHR/LOS000	NORTHR/LOS270	0.48	0.41	0.83
3	1602	DUZCE/BOL000	DUZCE/BOL090	0.82	0.73	0.63
4	1787	HECTOR/HEC000	HECTOR/HEC090	0.34	0.27	1.09
5	169	IMPVALL/H-DLT262	IMPVALL/H-DLT352	0.35	0.24	1.31
6	174	IMPVALL/H-E11140	IMPVALL/H-E11230	0.38	0.36	1.01
7	1111	KOBE/NIS000	KOBE/NIS090	0.51	0.50	1.03
8	1116	KOBE/SHI000	KOBE/SHI090	0.24	0.21	1.10
9	1158	KOCAELI/DZC180	KOCAELI/DZC270	0.36	0.31	0.69
10	1148	KOCAELI/ARC000	KOCAELI/ARC090	0.22	0.15	1.36
11	900	LANDERS/YER270	LANDERS/YER360	0.24	0.15	0.99
12	848	LANDERS/CLW-LN	LANDERS/CLW-TR	0.42	0.18	1.15
13	752	LOMAP/CAP000	LOMAP/CAP090	0.53	0.44	1.09
14	767	LOMAP/G03000	LOMAP/G03090	0.56	0.37	0.88
15	1633	MANJIL/ABBAR-L	MANJIL/ABBAR-T	0.51	0.50	0.79
16	721	SUPERST/B-ICC000	SUPERST/B-ICC090	0.36	0.26	0.87
17	725	SUPERST/B-POE270	SUPERST/B-POE270	0.45	0.44	1.17
18	829	CAPEMEND/RIO270	CAPEMEND/RIO360	0.55	0.39	0.82
19	1244	CHICHI/CHY101-E	CHICHI/CHY101-N	0.44	0.35	0.41
20	1485	CHICHI/TCU045-E	CHICHI/TCU045-N	0.51	0.47	0.96
21	68	SFERN/PEL090	SFERN/PEL180	0.21	0.17	2.10
22	125	FRIULI/A-TMZ000	FRIULI/A-TMZ270	0.35	0.31	1.44

probabilities in the common friction damper and structures with the hybrid damper becomes smaller. The reason of low effectiveness of hybrid damper in IO and LS damage states is directly related to geometry of hybrid friction damper. As mentioned before, the main fuse engaged in response of structure when the structure suffers high drift demand greater than 1% correspond to the life safety damage states. Before the structure experience the 1% drift demand, only auxiliary fuse of hybrid damper improves seismic response of structure while after this demand, both of main and auxiliary fuse enhance the responses. In summary, it is observed that the installation of the hybrid dampers appears to be the most effective in the collapse prevention damage state.

5 Conclusions

This paper dealt with introducing and experimenting a new kind of hybrid friction damper to provide two performance level during earthquakes. Also the comparative seismic assessment of 3- and 9-story steel moment resisting frames equipped with HFD dampers and conventional friction dampers using statistical and probabilistic analysis of

incremental nonlinear time-history analyses outputs under a large set of ground motion records.

In all experimented HFDs, the purpose of reaching dual performance level is achieved. The auxiliary fuse slips when displacement are less than 15 mm without involving the second fuse. After an increase in the applied displacement, the force transmission has been feasible through the connectors (bolts) to the second fuse and strength force of damper enhanced.

The HFD displacement-force characteristics such as slip load, dissipated energy, effective stiffness and equivalent viscous damping for cyclic loading calculated according to ASCE / SEI41-06 regulation. The results show that standard deviation of these values is within the 15% range in the load cycles. In the most critical case related to the first cycle of Sample B, the standard deviation of the slip load and energy dissipation values is 10% and 11%, respectively.

The results of numerical studies demonstrate that the numerical model using link element combination in Open Sees software is able to properly model the dual phase behavior of HFD. Also, reviewing the energy dissipation

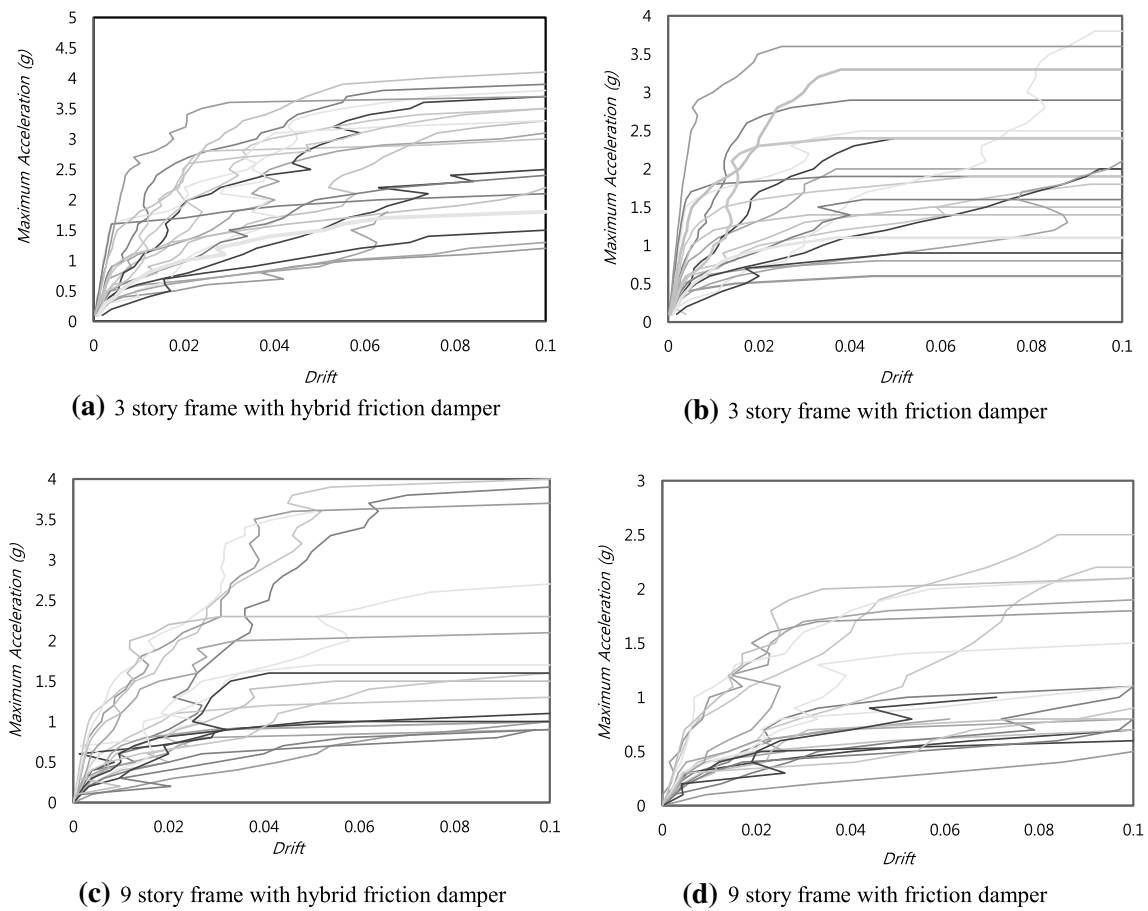


Fig. 17 Incremental dynamic analysis results of the model structures

during loading indicates that, by adding the main fuse to the energy dissipation system, energy dissipation increases significantly, in which the magnitude of the increase is proportional to the structural requirement in high-intensity earthquakes.

Results of incremental dynamic analysis showed remarkable reduction in important engineering demand parameters including the peak inter-story drift ratio for systems equipped with HFD dampers in contrast to the conventional

friction dampers. All the above enhancements stem from improvements in strength and hysteretic energy dissipation characteristics of the device and its intrinsic low stiffness degradation. Evaluation of the median IDA curves for 3 and 9 story frames showed, on average, 40% and 100% increase in probable PGA for collapse prevention limit state. It is generally evident that the effectiveness of HFD become more significant for the collapse prevention limit state.

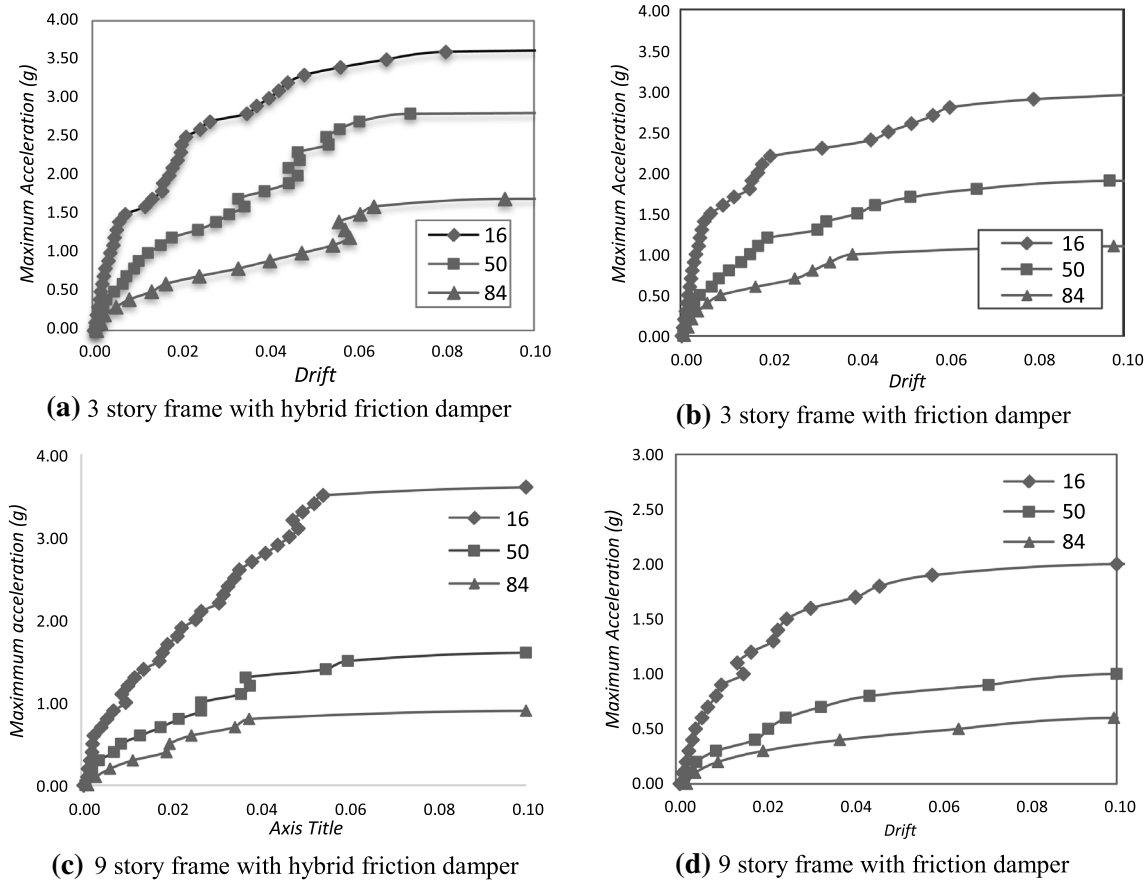


Fig. 18 Compact IDA curves for the model structures

Table 6 Summary of damage states of IDA curves (a) 3 story frames (b) 9 story frames

	3 story frame with friction damper						3 story frame with HDF					
	PGA			θ_{max}			PGA			θ_{max}		
	CP	LS	IO	CP	LS	IO	CP	LS	IO	CP	LS	IO
(a)												
16%	2.2	1.8	1.62	0.02	0.015	0.01	2.74	1.8	1.55	0.03	0.015	0.01
50%	1.3	1	0.8	0.02	0.015	0.01	1.8	1.1	0.9	0.039	0.015	0.01
84%	1	0.58	0.51	0.038	0.015	0.01	1.6	0.55	0.43	0.063	0.015	0.01
	9 story frame with friction damper						9 story frame with HDF					
	PGA			θ_{max}			PGA			θ_{max}		
	CP	LS	IO	CP	LS	IO	CP	LS	IO	CP	LS	IO
(b)												
16%	1.1	1.1	1	0.154	0.015	0.01	1.6	1.53	1.1	0.017	0.015	0.01
50%	0.5	0.47	0.41	0.018	0.015	0.01	1	0.74	0.62	0.027	0.015	0.01
84%	0.45	0.38	0.31	0.028	0.015	0.01	0.8	0.44	0.39	0.034	0.015	0.01

References

Andalib, Z., Kafi, M. A., Kheyroddin, A., & Bazzaz, M. (2014).

Experimental investigation of the ductility and performance of steel rings constructed from plates. *Journal of Constructional*

- Steel Research*, 103, 77–88. <https://doi.org/10.1016/j.jcsr.2014.07.016>
- Andalib, Z., Kafi, M. A., Kheyroddin, A., Bazzaz, M., & Momenzadeh, S. (2018). Numerical evaluation of ductility and energy absorption of steel rings constructed from plates. *Engineering Structures*, 169, 94–106. <https://doi.org/10.1016/j.engstruct.2018.05.034>
- ASCE/SEI 41-13. (2010). Seismic evaluation and retrofit of existing buildings. American Society of Civil Engineers; Reston, Virginia, USA.
- ASCE/SEI 7-10. (2010). Minimum design loads for buildings and other structures. American Society of Civil Engineers; Reston, Virginia, USA.
- Bazzaz, M., Andalib, Z., Kafi, M. A., & Kheyroddin, A. (2015). Evaluating the performance of OBS-CO in steel frames under monotonic load. *Journal of Earthquakes and Structures*, 8(3), 697–710. <https://doi.org/10.12989/eas.2015.8.3.699>
- Bazzaz, M., Kafi, M. A., Kheyroddin, A., Andalib, Z., & Esmaili, H. (2014). Evaluating the seismic performance of off-centre bracing system with circular element in optimum place. *International Journal of Steel Structures*, 14(2), 293–304. <https://doi.org/10.1007/s13296-014-2009-x>
- Bazzaz, M., Kheyroddin, A., Kafi, M. A., & Andalib, Z. (2012). Evaluation of the seismic performance of off-centre bracing system with ductile element in steel frames. *Steel & Composite Structures*, 12(5), 445–464. <https://doi.org/10.12989/scs.2012.12.5.445>
- BHRC. (2015). Iranian code of practice for seismic resistant design of buildings (Standard No. 2800) (4th ed.), Building Housing Research Center; Tehran, Iran.
- Cheraghi, A., & Zahrai, S. M. (2016). Innovative multi-level control with concentric pipes along brace to reduce seismic response of steel frames. *Journal of Constructional Steel Research*, 127, 120–135. <https://doi.org/10.1016/j.jcsr.2016.07.024>
- FEMA350. (2000). Recommended Seismic Design Criteria for New Steel Moment Frame Buildings, Federal Emergency Management Agency; Washington, DC, USA.
- FEMA356. (2000). Commentary for the seismic rehabilitation of buildings, Federal Emergency Management Agency 7; Washington, DC, USA.
- FEMA-P695 (2009). Quantification of building seismic performance factors, Report No. P695, Federal Emergency Management Agency; Washington, DC, USA.
- Hanson, R. D. & Soong, T. T. (2001). “Seismic design with supplemental energy dissipation devices”, *Oakland (CA): Earthquake Engineering Research Institute*.
- Hosseini, H. B., & Moaddab, E. (2017). Experimental study of a hybrid structural damper for multi-seismic levels. *Proceedings of the Institution of Civil Engineers-Structures and Buildings*, 170(10), 722–734. <https://doi.org/10.1680/jstbu.15.00122>
- Ibarra, L. F., Medina, R. A., & Krawinkler, H. (2005). Hysteretic models that incorporate strength and stiffness deterioration. *Earthquake Engineering & Structural Dynamics*, 34, 1489–1511. <https://doi.org/10.1002/eqe.495>
- Ibrahim, Y. E., Marshall, J., & Charney, F. A. (2007). A visco-plastic device for seismic protection of structures. *Journal of Constructional Steel Research*, 63(11), 1515–1528. <https://doi.org/10.1016/j.jcsr.2007.01.007>
- Karavasilis, T. L., Blakeborough, T., & Williams, M. S. (2011). Development of nonlinear analytical model and seismic analyses of a steel frame with self-centering devices and viscoelastic dampers. *Computers & Structures*, 89(11–12), 1232–1240. <https://doi.org/10.1016/j.compstruc.2010.08.013>
- Kim, D. H., Ju, Y. K., et al. (2009). Experimental Study on the Vibration Control Capacity of Hybrid Buckling-Restrained Braces. *Journal of Korean Society of Steel Construction*, 21(1), 83–91.
- Kim, D. H., Ju, Y. K., Kim, M. H., & Kim, S. D. (2014). Wind-induced vibration control of tall buildings using hybrid buckling-restrained braces. *The Structural Design of Tall and Special Buildings*, 23(7), 549–562. <https://doi.org/10.1002/tal.1066>
- Lee, C.-H., Kim, J., et al. (2016). Numerical and experimental analysis of combined behavior of shear-type friction damper and non-uniform strip damper for multi-level seismic protection. *Engineering Structures*, 114, 75–92. <https://doi.org/10.1016/j.engstruct.2016.02.007>
- Marshall, J. D., & Charney, F. A. (2010). A hybrid passive control device for steel structures, I: Development and analysis. *Journal of Constructional Steel Research*, 66(10), 1278–1286. <https://doi.org/10.1016/j.jcsr.2010.04.005>
- Mazzoni, S., & McKenna, F., et al. (2006). “OpenSees command language manual.” Pacific Earthquake Engineering Research (PEER) Center 264.
- OpenSees (2014). The Open System for Earthquake Engineering Simulation. Pacific Earthquake Engineering Research Center (PEER). Available at: <http://opensees.berkeley.edu>
- Smith, R. J., & Willford, M. R. (2007). The damped outrigger concept for tall buildings. *The Structural Design of Tall and Special Buildings*, 16(4), 501–517. <https://doi.org/10.1002/tal.413>
- Soong, T., & Spencer, B. (2002). Supplemental energy dissipation: State-of-the-art and state-of-the-practice. *Engineering Structures*, 24(3), 243–259. [https://doi.org/10.1016/S0141-0296\(01\)00092-X](https://doi.org/10.1016/S0141-0296(01)00092-X)
- Symans, M., Charney, F., et al. (2008). Energy dissipation systems for seismic applications: Current practice and recent developments. *Journal of Structural Engineering*, 134(1), 3–21.

Publisher's Note Springer Nature remains neutral with regard to jurisdictional claims in published maps and institutional affiliations.